RESEARCH ARTICLE

Functional Anatomy of the Fiddler Crab Compound Eye (*Uca vomeris:* Ocypodidae, Brachyura, Decapoda)

Ali Alkaladi, and Jochen Zeil*

ARC Centre of Excellence in Vision Science, Research School of Biology, Australian National University, Canberra, Australia

ABSTRACT

We describe the structural organization of the ommatidium in the compound eye of the fiddler crab, *Uca vomeris*, at both the light- and the electron-microscopy levels. We pay particular attention to the organization of the optical system, the retinular cells, the rhabdom, and of pigment cells. Although the fiddler crab compound eye is of the apposition type, typical for Brachyuran crabs, we identify a number of novel, functionally relevant aspects of ommatidial organization that have not previously been described. The flat corneal facet lenses provide the main focusing power and therefore must contain a gradient of refractive index. Each ommatidium has the typical set of eight retinular cells, with a distal retinular cell R8 lying close to the proximal tip of the crystalline cone. R8 is shaped into four lobes, which are separated by proximal extensions of the four crystalline cone cells and of distal extensions of retinular cells R1–R7. The microvilli in the R8 rhabdom are not aligned in a uniform direction, while the microvilli of the main rhabdom show the typical crustacean pattern of alternating bands of horizontally (R3, R4, R7) and vertically aligned microvilli (R1, R2, R5, R6). We describe in detail the distribution and structural properties of screening pigment granules in the two types of pigment cells and in the retinular cells in the equatorial eye. We discuss the functional significance of this fine-structural organization of the fiddler crab compound eye in relation to visual processing and visual ecology. J. Comp. Neurol. 522:1264–1283, 2014.

INDEXING TERMS: Crustacea; *Uca vomeris*; compound eye; ommatidium; retinular cells; rhabdom; screening pigments; visual ecology

At present, around 100 species and subspecies of fiddler crabs (Genus *Uca*) have been identified worldwide (Crane, 1975; Rosenberg, 2001). Fiddler crabs live in tropical mud or sand flats, and, with few exceptions, are active during diurnal low tides. The crabs are famous for the sexual dimorphism of claw size (Crane, 1975): females have small, same-sized feeding claws, while males have one claw that is massively enlarged. The males use their large claw as a signaling device in waving displays and as a weapon in fights with other males (Crane, 1975; Pope, 2005). Fiddler crabs carry their eyes on long vertical stalks, and the eyes have a panoramic visual field. In addition, resolution varies across the visual field (Zeil et al., 1986; Land and Layne, 1995; Zeil and Al-Mutairi, 1996; Smolka and Hemmi, 2009). Fiddler crabs are very visual animals, which employ a variety of visual signals from claw-waving displays to brilliant body colors (reviewed in Zeil and Hemmi, 2006). However, very little is known about the detailed properties of fiddler crab compound eyes. The crabs have apposition eyes, and the most noticeable feature of them is the varying dimensions of ommatidia across the visual field (Land and Layne, 1995; Zeil and Al-Mutairi, 1996). At the eye equator, the lenses are larger, and the crystalline cones and rhabdoms are longer than in the dorsal and ventral part of the compound eye. This indicates that light sensitivity and resolution differ in different parts of the eye. The resolving power in the compound eyes of the species of fiddler

Present address for Ali Alkaladi: Department of Biological Sciences, Faculty of Science, North Campus, King Abdulaziz University, PO Box 11508, Jeddah 21463, Saudi Arabia.

Grant sponsor: Australian Research Council Centre of Excellence Scheme; Grant number: CEO561903; Grant sponsor: Ministry of Higher Education in Saudi Arabia; Grant sponsor: Vice President for Educational Affairs of King Abdulaziz University.

*CORRESPONDENCE TO: Jochen Zeil, ARC Centre of Excellence in Vision Science, Research School of Biology, Australian National University, Biology Place, Bldg. 46, Canberra, ACT 0200, Australia.
E-mail: jochen.zeil@anu.edu.au

Received April 8, 2013; Revised September 16, 2013;
Accepted September 17, 2013.
DOI 10.1002/cne.23472
Published online October 1, 2013 in Wiley Online Library (wileyonlinelibrary.com)

crabs that have been studied so far (*Uca flammula*: Zeil et al., 1986; *Uca pugilator:* Land and Layne, 1995; *Uca lactea annulipes*: Zeil and Al-Mutairi, 1996; *Uca vomeris*: Smolka and Hemmi, 2009) is the highest along the eye equator and differs between the dorsal and the ventral visual fields. Because eyes are raised high above the body and because the crabs live in locally very flat terrain, the visual world of fiddler crabs is divided into distinct zones of visual information: ommatidia in the ventral and equatorial eye see other crabs, while the ommatidia in the dorsal eye see predators such as birds (Smolka and Hemmi, 2009). Everything larger than the crabs themselves is seen above the line of horizon (Zeil et al., 1986; Zeil and Al-Mutairi, 1996; Layne et al., 1997; Layne, 1998). Although we know the distribution of resolving power of these highly specialized eyes from *in vivo* optical studies, we are ignorant about important details of their functional anatomy, which is crucial for our understanding of how these eyes sample the visual world (e.g., Zeil and Zanker, 1997; Zeil and Hofmann, 2001; Smolka et al., 2011; reviewed in Zeil and Hemmi, 2006; Hemmi and Tomsic, 2011).

To date, there has been no fine-structural analysis of fiddler crab eyes, with the exception of two electron micrographs of the rhabdom in Shaw and Stowe (1982) and a recent analysis of microvillar banding patterns by Alkaladi et al. (2013). In *Ocypodid* and *Grapsid* crabs, histological studies have focused on the position of the distal eighth retinular cell R8 (Dembowski, 1913; Kunze, 1967) and on the dramatic size changes of the rhabdom between day and night (Kunze and Boschek, 1968; Waterman, 1981; Stowe, 1982; Toh, 1987; Rosenberg et al., 2001; Rosenberg and Langer, 2001), providing at least some information on the functional anatomy of the whole eye (e.g., for the ghost crab, *Ocypode,* in Rosenberg et al., 2001).

Here we present the first comprehensive description of the functional anatomy of the fiddler crab ommatidium, paying particular attention to the dimensions and relative positions of the optical train, the rhabdom and of screening pigments.

MATERIALS AND METHODS

Animals

Adult male and female *U. vomeris* were collected at Keppel Sands, north of Rockhampton, Queensland, Australia. Live animals were transported in a Styrofoam cooler over 2 days by car to the Australian National University where they were kept at natural daily changes of illumination in plastic containers filled to about 0.5 cm with seawater, containing a piece of tissue paper. The crabs were fed flakes of fish and had acclimatized for 1 week before being prepared for histology.

Development of preparation methods

Eyes were prepared for light- and electron-microscopy using standard procedures. We had to develop new ways of prefixation preparation of the eyes because the cuticle of the eye stalks is very hard and a way needed to be found to allow fixative to reach the eye tissue as quickly as possible to make sure that all parts of the eye were sufficiently well preserved. The method we finally settled on was to anesthetize animals by cooling for 3–4 minutes in the deep freeze compartment of a refrigerator and to use medical surgery knives (Super Sharps Microsurgical Knives, MSP, UK), dipped in fixative, to make a cut along the medial cuticular ridge running between the anterior and posterior part of the eye, while the eye rested in the horizontal orbital grooves running along the dorsal-frontal carapace. The eye stalk was subsequently cut, still supported by the orbital grooves, by making a deep incision perpendicular to the long axis of the orbital groove and the eye stalk as close as possible to the eye. The orbital groove was flushed with fixative, before the eye was collected with forceps and immersed in fixative. Animals were immediately killed by placing them on dry ice. We found that the method of initial surgery affects the presence and color of screening pigments, some of which could not be detected using the standard procedure of simply cutting the eye stalks as close to the eyes as possible. Also, the preservation of microvilli was greatly improved by this preparation method.

Histological procedure

Since *U. vomeris* in Australia are exclusively active during diurnal low tides, eyes were prepared for histology in the fully light-adapted state between 8:30 and 11:00. Eyes were fixed for 2–4 hours at room temperature in a mixture of 2.5% glutaraldehyde and 3.7% formaldehyde in seawater and subsequently washed in three changes of seawater for 10 minutes each. Postfixation occurred in 1% OsO_4 (osmium) in distilled water for 2 hours, followed by three 15-minute washes in distilled water. The eyes were dehydrated through a sequence of 70%, 80%, 90%, 95%, and 2$\times$ 100% ethanol for 15 minutes each and infiltrated with resin (Araldite 502) through a mixture of pure propylene oxide for 1 hour, 25/75 resin/propylene oxide for 2 hours, 50/50 resin/propylene oxide (overnight), followed by 75/100 resin/propylene oxide for 2 hours and pure resin for at least 6 hours before embedding them and curing the plastic at 60°C for 24 hours. The crabs used in this study had male carapace widths of 1.70, 2.30. 2.32, 2.90 (n = 4) and female carapace widths of 2.26 and 2.44 cm ($n = 2$). The data we present here are mainly from male crabs.

For light microscopy, the tissue was sectioned at 1 or 2 μm. Serial sections were cut on an ultramicrotome using glass and diamond knives (Diatome Histo Jumbo) and stained with Toluidine Blue. Intermittently, 0.01–0.1 μm sections cut with diamond knives were collected for electron microscopy, which were mounted on grids and stained with uranyl acetate and lead citrate. For light microscopy, we used Zeiss and Leitz microscopes and a Power Shot S50 Canon digital camera (5.0 Megapixels) with a custom-made eyepiece and phototube mount. For electron microscopy we used a Hitachi H7100FA (125 kv TEM, 1995) electron microscope with an integrated Megaview111 soft imaging system (SIS) digital camera to photograph ultrathin sections.

Hanging drop experiments

We carried out hanging drop experiments following the procedure described in Warrant et al. (2006) to test whether the cuticle lens or the crystalline cone provide the focusing power in the fiddler crab eye. We dissected out the cornea using medical surgical knives, removed the retina, and very gently cleaned the surfaces of the lenses using a soft paintbrush. Pieces of cornea from the dorsal, the equatorial, and the ventral part of the eye were transferred to a small drop of seawater on a glass coverslip taking care that the outside surface of the corneal lenses faced air and the inside surface the drop of water. The coverslip was inverted and placed on an O-ring on a microscope side. An object was then placed above the imaging field diaphragm in the illumination light path in the foot of the microscope, the condenser of which had been removed, at a distance of about 10 cm from the specimen. The object consisted of a checker board pattern of black and translucent squares, printed on a transparency, with square size 1 mm. We then determined the distance between the back of the lens and the best focused image of the pattern (the back focal plane of the lens), using a micro gauge placed on the microscope stage. Because the microscope objective is in air and the specimen was in seawater the measurements were corrected by multiplying them by the refractive index of seawater ($n = 1.34$).

Retinular cell numbering convention

Different ways of numbering the retinular cells R1–R7 in crustaceans have been used in the literature as discussed in detail by Shaw and Stowe (1982, footnote p. 327). In addition, some confusion has arisen because the cellular components of ommatidia are arranged mirror-symmetrically in the dorsal and the ventral and the left and the right eye (see schematic drawing in Fig. 8I). For published cross-sections and schematic diagrams, it is not always clearly stated whether they represent the situation in the left or the right eye and/or from the dorsal or the ventral part of the eye. We use here the original numbering system introduced by Parker (1897) that assigns R7 (and not R1) to the large unpaired retinular cell (see Fig. 8I). Besides the historical precedence of this numbering system, there is now also strong evidence from developmental studies that the unpaired retinular cells R7 and R8 in crustaceans are homologous to the unpaired insect retinular cells R7 and R8 (Ready, 1989; Meinertzhagen, 1991; Melzer et al., 1997, 2000; Hafner and Tokarski, 2001; Harzsch and Hafner, 2006; Friedrich et al., 2011).

RESULTS

General description of the *U. vomeris* compound eye

Uca vomeris carry their eyes on long vertically held stalks (top row Fig. 1). Each compound eye is made up of more than 9,000 ommatidia (Smolka and Hemmi, 2009). The eyes are elongated in the vertical direction and are bordered on the medial side by a narrow cuticular ridge, which carries two, possibly mechanosensory hairs (Fig. 1). On the level of the following analysis, we did not find differences between male and female eyes.

The shape of the fiddler crab eye, as seen from the outside, shows that the local eye radius differs significantly in different parts of the eye (Fig. 1A). The local eye radius is large at the equatorial part of the eye and small in the dorsal and the ventral eye. The dimensions of ommatidial components vary greatly throughout the eye of *U. vomeris* (Fig. 1A,B), as has been reported previously for *Uca lactea annulipes* (Zeil and Al Mutairi, 1996) and, as far as facet diameters are concerned, for *U. vomeris* (Smolka and Hemmi, 2009). The longitudinal section in Figure 1A shows that the diameter of the lenses, the length of crystalline cones, and the length of the rhabdoms are largest in the equatorial eye. For a male of carapace width 2.15 cm, facet lenses are larger at the eye equator with diameters of about 36 μm, compared with 19 μm in the dorsal and 23 μm in the ventral part of the eye. Crystalline cones and rhabdoms are longer at the eye equator compared to the dorsal and ventral part of the eye (Fig. 1B). Rhabdoms at the frontal eye equator reach lengths of about 230 μm, compared with 100 μm at the dorsal and 60 μm at the ventral edge of the eye (Fig. 1B). In Figure 1C we calculated what consequences these variations have for the resolving power of the eye (see also Smolka and

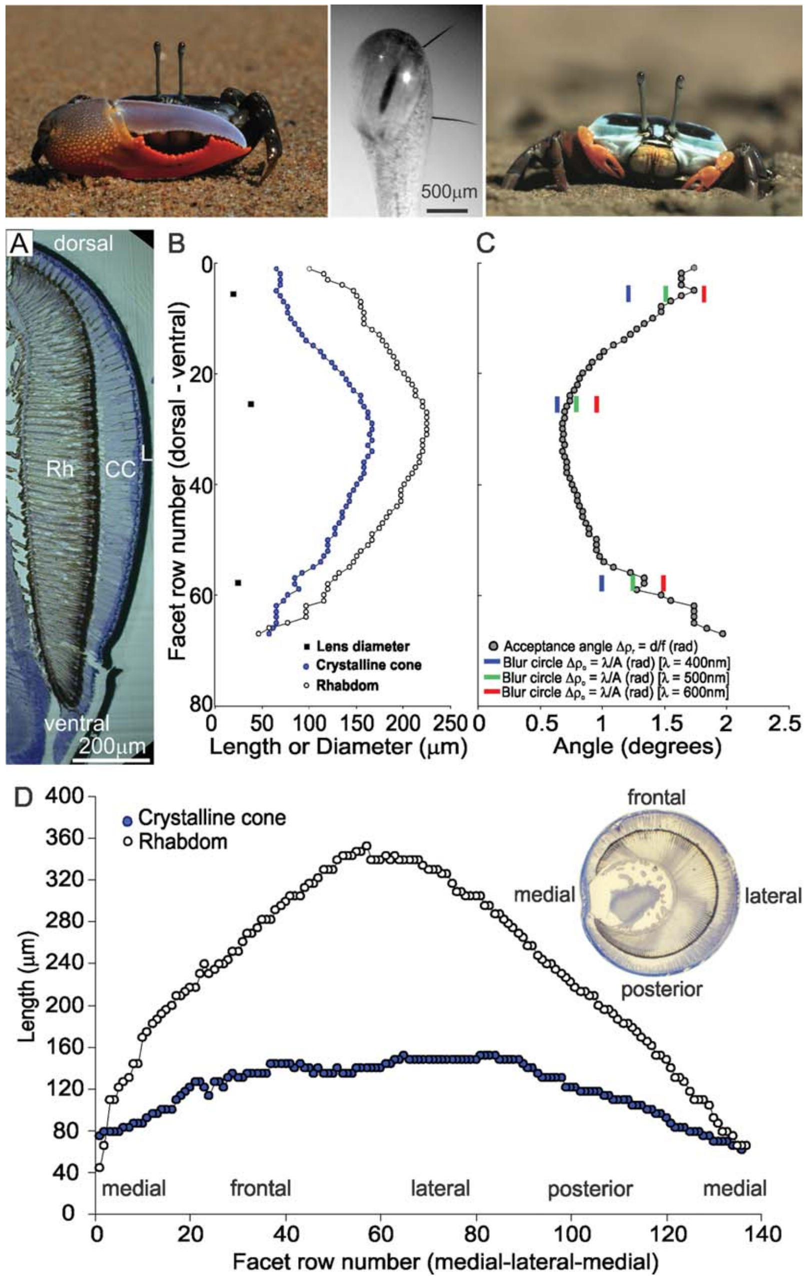

Figure 1. Overview of the *U. vomeris* compound eye. Top row images: *U. vomeris* male (left) and female (right). The photograph in the center shows the black pseudopupil in the frontal eye at the eye equator and the two medial hairs. **A:** Light micrograph of a sagittal section through the frontal eye of a female, carapace width 2.15 cm. L: Lenses; CC: Crystalline cones; Rh: Rhabdoms. **B:** Variation of anatomical dimensions from the dorsal to the ventral parts of the eye. The graph shows the length of crystalline cones (blue circles), the length of rhabdoms (open circles), and in three places the diameter of facet lenses (black squares) plotted according to the ommatidial row number (y-axis) from the most dorsal (facet row 0) to the most ventral part of the eye (facet 67). **C:** The optical consequences of these variations. The acceptance angle of the rhabdom (open circles), assuming a rhabdom diameter of 2 μm, is plotted according to dorsal to ventral ommatidial row number (y-axis), together with the half-width of the lens blur circle at three locations for monochromatic light of wavelengths 400 nm (blue), 500 nm (green) and 600 nm (red). (D) The variation of ommatidial dimensions in azimuth direction along the eye equator from fronto-medial (x-axis, facet row 0) to posterior-medial (facet row 138). Inset shows a light micrograph of the horizontal section through the equatorial part of the eye that was used to make these measurements. Blue circles: Length of crystalline cones; Open circles: Length of rhabdoms.

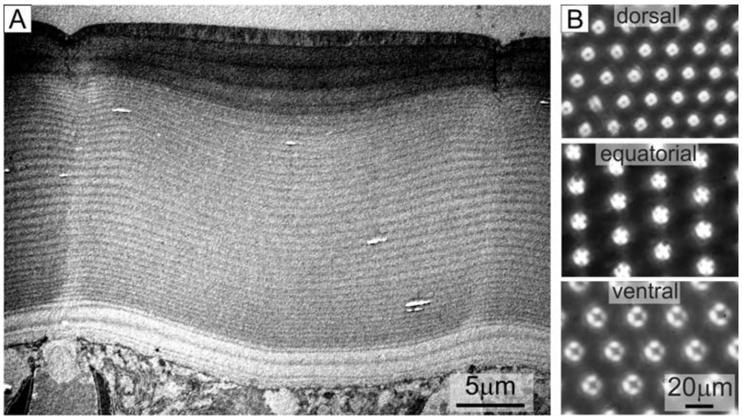

Figure 2. The properties of the *U. vomeris* facet lens. **A:** Electron micrograph of a longitudinal section through the lens showing layers of different densities in the lens and that the lens surface is flat. Male, carapace width 2.30 cm. **B:** Images of a test pattern produced by lenses in the dorsal eye (top) at a mean distance of best focus of 137 μm ($n = 6$) from the back of the lens, at the eye equator (middle) at a mean distance of best focus of 170 μm ($n = 6$), and in the ventral part of the eye at a mean distance of best focus of 136 μm ($n = 6$).

Hemmi, 2009). We estimated the rhabdom acceptance angle ($\Delta\rho_r = d/f$ (rad)), assuming a constant rhabdom diameter d of 2 μm and the focal length f to be equal to the length of the crystalline cone. We show in addition the half-width diameter of the blur circle ($\Delta\rho_l = \lambda/A$ (rad)) for three locations in which we measured the lens diameter (colored dots in Fig. 1C) and for three wavelengths λ, as indicated in the figure. Resolution is clearly highest and matched to shorter wavelengths in the equatorial, compared to the dorsal and ventral part of the eye (for a more comprehensive analysis, see Smolka and Hemmi, 2009).

Horizontal sections through the eye equator show that ommatidial dimensions also vary in azimuth directions (Fig. 1D). Crystalline cones and rhabdoms are longest in the lateral eye with 150 μm and 350 μm, respectively. The length of crystalline cones increases from 75 μm medially, through 120 μm frontally, to their maximal length of 150 μm in the lateral eye. Crystalline cones then decrease to 110 μm in the back and 65 μm in the posterior medial part of the eye. The rhabdom length increases from 80 μm frontomedially, through 230 μm frontally to their maximal length of 350 μm in the lateral eye. Rhabdom length decreases to 180 μm in the back and 65 μm in the posterior medial part of the eye.

Optics: lens and crystalline cone

Electron microscopy sections show that the lenses in *U. vomeris* are flat, not convex like in many terrestrial arthropods (Fig. 2A), indicating that focusing has to be achieved by a refractive index gradient either in the lens itself or in the crystalline cone, because a flat lens surface does not provide focusing power. To test whether the cuticle lens or the crystalline cone provide focusing in the fiddler crab ommatidium, we investigated the imaging properties of the lenses on their own by the hanging drop technique (see Materials and Methods for details).

During dissection, we did not find any intact crystalline cones, indicating that they are very soft. This is a first hint that the crystalline cone is not involved in focusing. We found that the corneal facet lenses in fiddler crabs are sufficient to focus light because the lenses themselves produce an image (Fig. 2B) at distances of best focus from the back surface of the lens at approximately the level of distal rhabdom tips in the intact eye, for cornea from the dorsal eye (120–140 mm), the eye equator (150–170 mm), and the ventral eye (117–148 mm). There thus must be a gradient of refractive index inside the lenses. The lens shows distinct bands of material at high and low density (Fig. 2A), but whether this density gradient indicates a gradient of refractive index is presently not clear (e.g., Nilsson, 1990) and needs to be confirmed by interference microscopy.

The eucone crystalline cone of the fiddler crab ommatidium is made up of four cone cells or semper cells flanked by two corneagenous cells (Fig. 3A). The nuclei of the four crystalline cone cells lie far distal, close to the cuticular lens (Fig. 3B). Between the crystalline cones the profiles of six distal or secondary pigment cells (also referred to as interommatidial pigment cells (Rosenberg et al., 2001)) form a hexagonal lattice (Fig. 3C). In the dorsal part of the compound eye,

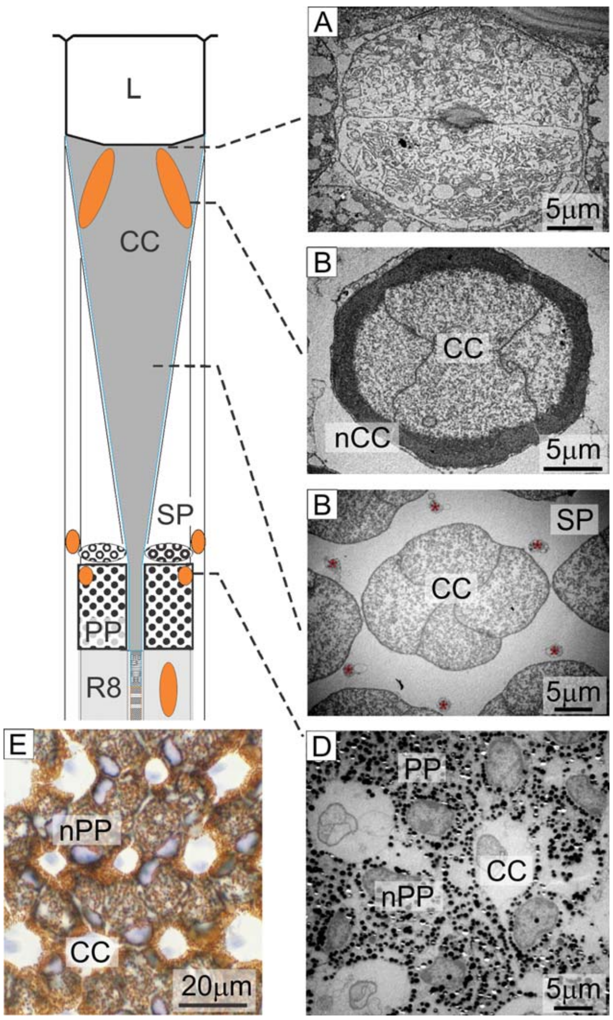

Figure 3. The crystalline cone of *U. vomeris*. Schematic drawing shows the optical tract from lens to rhabdom. Nuclei of different cellular components are shown in orange. L: Lens; CC: Crystalline cone; SP: Secondary pigment cells; PP: Primary pigment cells; R8: Distal retinular cell R8. **A:** The distal part of the crystalline cone with corneagenous cells anchoring the crystalline cone to the lens. **B:** Cross-section through the nuclear region (nCC) of the four crystalline cone cells (CC). **C:** Profiles of six secondary pigment cells (also referred to as inter-ommatidial pigment cells), marked by stars between the distal parts of crystalline cones (CC). **D:** Proximal tips of crystalline cones (CC) are surrounded by the dense pigment screen formed by six primary pigment cells (PP) around the proximal tip of the crystalline cone and the distal tip of the rhabdom. nPP: nuclei of primary pigment cells. **E:** Light micrograph cross-section through the primary pigment cell layer. Male, carapace width 1.7 cm.

secondary pigment cells form thin pigment screens between the crystalline cones, as we will describe in detail below. The crystalline cone tapers towards the distal tip of the rhabdom. Just before reaching the rhabdom, the proximal tip of the crystalline cone is tightly surrounded by a dense pigment screen formed by the six proximal pigment cells (Fig. 3D,E).

Distribution of screening pigments in pigment cells

As in other crustacean eyes, the cellular components of the fiddler crab ommatidium include two classes of pigment cells, distinguished by their distal and proximal location in the ommatidium. There is no unified nomenclature for these pigment cells in the literature, with some authors calling them distal and proximal pigment cells (e.g., Arikawa et al., 1987), others distal and interommatidial pigment cells (e.g., Hallberg and Elofsson, 1989; Rosenberg et al., 2001), or primary and secondary pigment cells (Shaw and Stowe, 1982). We will use here the latter terminology. The secondary (distal) pigment cells extend from the level of the cuticular lenses, where they appear to be anchored at the inner indentation between facets, to the primary (proximal) pigment cell layer that surrounds the proximal tips of crystalline cones.

In the equatorial eye, the thin extensions of secondary pigment cells between the crystalline cones are free of pigment granules; the pigment cells are T-shaped and form long processes running between crystalline cone tips in a vertical (dorsoventral) direction parallel and just distal to the primary pigment cell layer (Fig. 4A,B). The secondary pigment cell extensions give rise to multicolored pigment bodies distal to the black primary pigment cell layer, which contain diverse pigment granules (Figs. 4C,D, 5). The spindle-shaped nuclei of secondary pigment cells lie in these basal cell extensions (Fig. 4D–F). The pigment granules in these multicolored pigment bodies are of very different sizes, shapes, and electron-densities (Fig. 5), ranging in size from submicron dimensions to over 1 micron (Fig. 5C). Some pigment granules appear empty viewed in the electron microscope with a diameter of about 0.3 μm. In contrast, some of the larger pigment granules are very electron-dense, but not as dense as the pigment granules in the primary pigment cells (inset, Fig. 5C) and in the retinular cells (see below). Such diversity of pigment granules is not seen in any other cellular component of the fiddler crab compound eye.

In the dorsal part of the eye, however, secondary pigment cells are modified to form pigment screens between crystalline cones (Fig. 6A). The spindle-shaped nuclei of secondary pigment cells are located distally between the crystalline cones and are surrounded by electron-dense pigment granules (Fig. 6H). Towards the equatorial part of the eye there is a distinct change in secondary pigment cell morphology. This change is marked by the change in location of the secondary pigment cell nuclei (Fig. 6B), which now come to lie proximally, just distal to the primary pigment cell layer (PP). The secondary pigment cell profiles between the crystalline cones are accompanied by cell profiles containing pigment granules (Fig. 6C,D,F,G). These

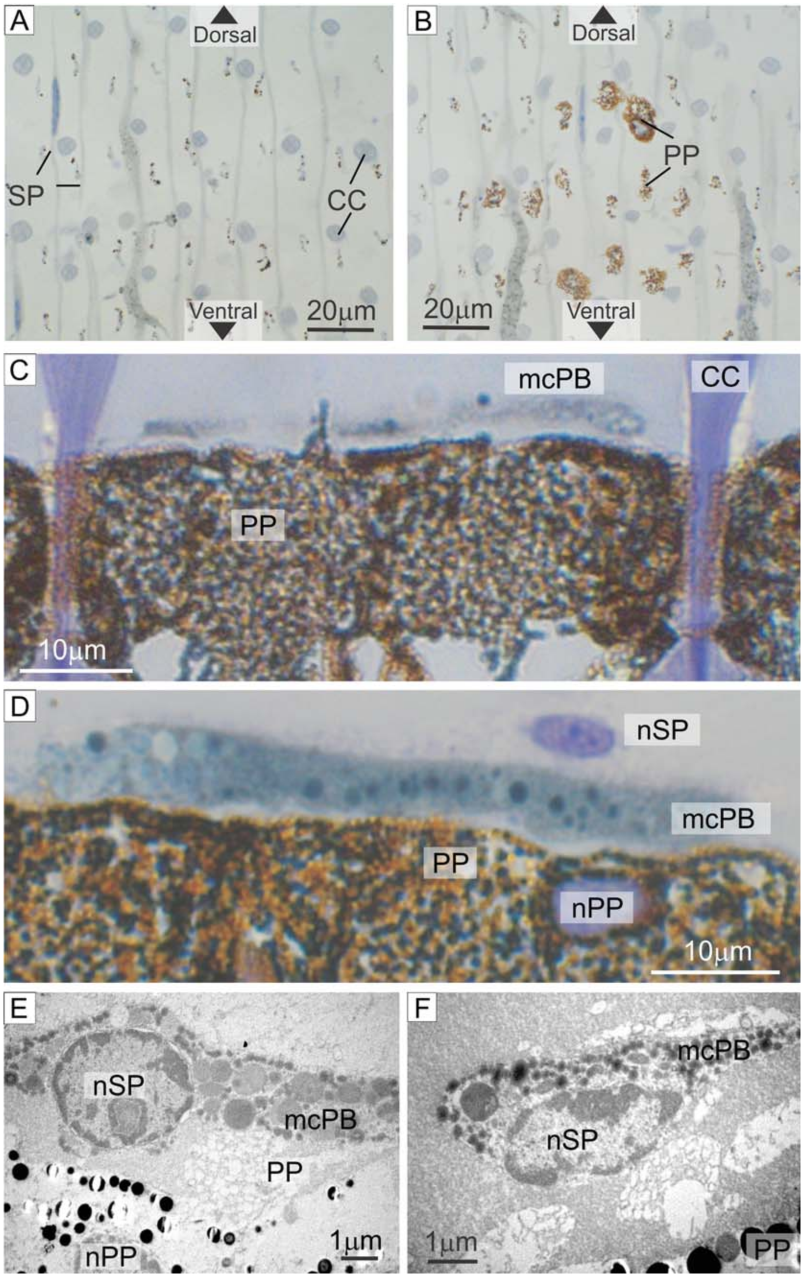

Figure 4. The secondary pigment cells at eye equator of *U. vomeris*. **A:** Secondary pigment cell profiles at the eye equator (SP) run in a dorsoventral direction between the proximal crystalline cone tips (CC), just distal to the primary pigment cell layer (PP), the golden-orange color of which can be seen in **(B)**. Male, carapace width 1.70 cm. **C:** Light micrograph of longitudinal sections showing multicolored pigment compartments (mcPB) between crystalline cone tips (CC), just distal to the primary pigment cell layer (PP). **D:** Light micrograph showing the location of nuclei of secondary pigment cells (nSP) and primary pigment cells (nPP). **E:** Electron micrograph of a longitudinal section through a secondary pigment cell compartment just above the primary pigment cell layer. nPP: Nucleus of primary pigment cell; nSP: Nucleus of secondary pigment cell; mcPB: Multicolored pigment body. **F:** The nuclei of secondary pigment cells (nSP) are embedded in multicolored pigment compartments (mcPB) and lie just distal to the primary pigment cell layer (PP). Male, carapace width 2.30 cm.

pigment-containing profiles are formed by a part of the secondary pigment cells, which is folded back running from distal to proximal parallel to the microtubule-rich secondary pigment cell profiles (Fig. 6C,F,G). In the dorsal part of the eye, the proximal ends of secondary pigment cells are shaped into a tight cup anchored around distal pin-like extensions of the primary pigment cells (Fig. 6I,J). Thus, in the dorsal part of the eye, the thin extensions of secondary pigment cells that lie parallel to the long axis of crystalline cones form pigment

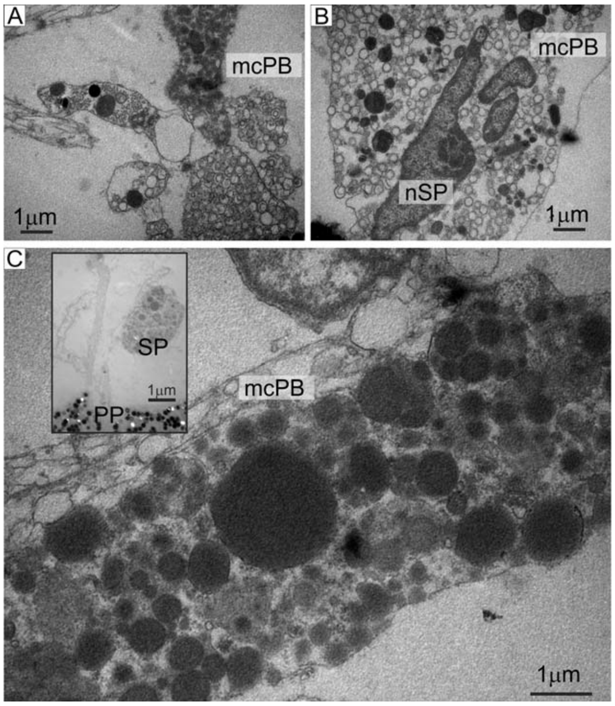

Figure 5. Secondary pigment cell granules at the eye equator of *U. vomeris*. **A:** electron micrograph of a section through two kinds of multicolored pigment compartments. **B:** The nuclei of secondary pigment cells (nSP) are embedded in these compartments (mcPB). **C:** High-magnification EM section showing the diversity of sizes, shapes, and electron densities of pigment granules in multicolored pigment compartments (mcPB). Inset shows position of these compartments just distal to the primary pigment cell layer with very electron-dense pigment granules. Male, carapace width 2.3 cm.

compartments (Fig. 6D), while these extensions are pigment-free in the rest of the eye (Fig. 6E).

The six primary pigment cells form a dense tangential pigment screen just distal to where the crystalline cone and the rhabdom meet (Fig. 7A,B). The pigment screen appears golden and black when viewed in the light microscope and contains a mixture of black, electron-dense and gray, less electron-dense pigment granules of about the same shape and size (Fig. 7C). At the crystalline cone–rhabdom interface, primary pigment cell granules retreat from the center of the ommatidium and form a pigment screen around the outside of the retinular cells (Fig. 7D–F). Long, single-row pigment granule strands originate from this primary pigment screen around each ommatidium and form a regular network of pigmented sheets between ommatidia (Fig. 7G,H).

Organization of the retinular cells and the rhabdom

Fiddler crabs have the typical crustacean arrangement of eight retinular cells with retinular cell R8 forming the distal part of the rhabdom, meeting the proximal tip of the crystalline cone and sitting on top of the main rhabdom formed by retinular cells R1 to R7 (see schematic drawing in Fig. 8A and longitudinal section in Fig. 8B; cell numbering according to Shaw and Stowe (1982); see Fig. 8I). The rhabdom of R8 has a diameter of about 1 μm (Fig. 8C,D; 0.9 ± 0.1 [n = 17]) and its length, as estimated by measuring the distance between the nucleus of R8 to the nuclei of R1–R7 (see Fig. 8B) is in the equatorial part of the eye 28.0 ± 3.6 μm (n = 5), compared to the length of the main rhabdom of 201.2 ± 5.7 μm (n = 5). The diameter of the main rhabdom (R1–R7) is ~1.5 μm (Fig. 8F, 1.6 ± 0.2 [n = 12]). The nuclei of R8 retinular cells are large, round, and are located close to the proximal edge of the primary pigment cells layer (Fig. 8B). In vertical cross-sections, the location of the R8 nucleus within each ommatidium provides a convenient landmark that defines the eye equator (Fig. 8G): R8 nuclei are displaced dorsally with respect of the central ommatidial axis in the dorsal part of the eye and ventrally in the ventral part of the eye, which corresponds to the general pattern found in ocypodid crabs (Kunze, 1967).

Retinular cells R1–R7 form the main rhabdom, which stretches from the level of R1–R7 nuclei just proximal of R8 to the basement membrane (Fig. 8B). The nuclei of R1–R7 have an oval shape in longitudinal sections (Fig. 8B) and lie all in one plane (Fig. 8H). The transition from R8 to the main rhabdom occurs at the level of R1–R7 nuclei and is marked by a widening of the perirhabdomal palisade vacuole (Fig. 8E,F).

In electron microscopy cross-sections, desmosomes mark the corners where the cell membranes of different cells meet, which allowed us to identify the origin of different cell profiles. We will first describe the architecture of retinular cell R8, before turning to the arrangement of retinular cells R1 to R7. A general overview of cross-sections through the ommatidium of *U. vomeris* at different levels along the length of the ommatidium is shown in Figure 9. Note in particular the difference in the distribution of screening pigment in R8 (Fig. 9A,B) and in R1–R7 (Fig. 9C–H). We will give a detailed account of this distribution later.

At the level of the nucleus, the cell body of R8 has a four-lobed shape (e.g., Dembowski, 1913; Kunze, 1967; Eguchi and Waterman, 1973). We denote these four lobes by letters a to d (see Figs. 9A, 10). The lobes are separated by four flat extensions of the crystalline cone cells, three of which are visible in Figure 10A and are marked by a white star. These cone extensions (marked by arrows in Fig. 10D) form a barrier between the distal extensions of retinular cells R1–R7 and the rhabdom at

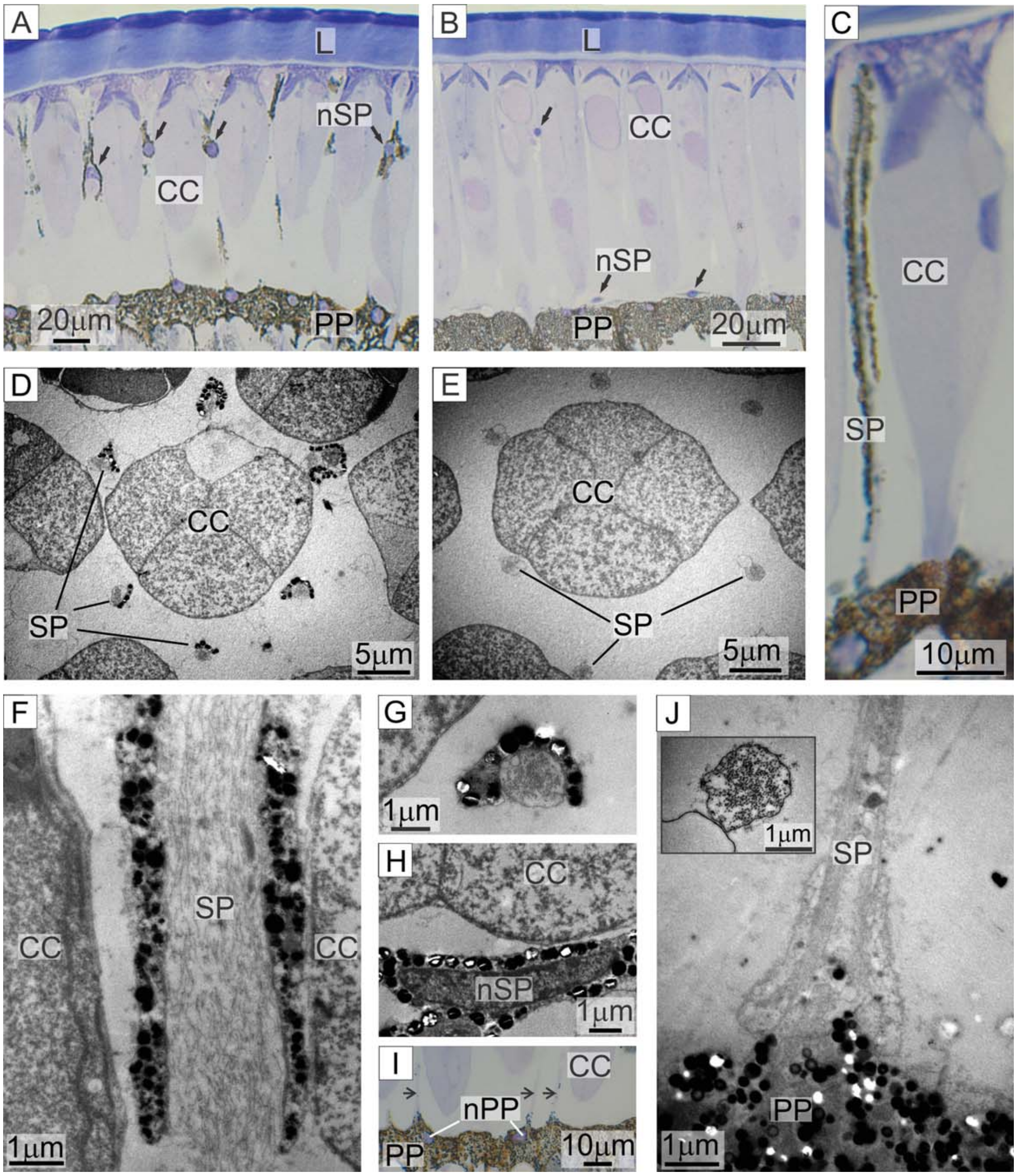

Figure 6. Regional variation in the secondary pigment cells of *U. vomeris*. **A:** Light micrograph of a longitudinal section through crystalline cones (CC) and primary pigment cell layer (PP) in the dorsal eye. The nuclei of secondary pigment cells (nSP, arrows) lie between the distal parts of crystalline cones. **B:** At the transition from equatorial (right) to dorsal eye (left), the nuclei of secondary pigment cells (nSP) change position from a proximal location close to the primary pigment cell layer in the equatorial and ventral eye to a far distal location towards the lenses between the crystalline cones. **C:** Longitudinal section through the secondary pigment cell screens (SP) between the distal crystalline cones (CC) in the dorsal eye. **D:** In the dorsal eye, distal extensions of secondary pigment cells (SP) give rise to compartments filled with black pigment granules. **E:** In the equatorial and ventral eye, the distal extensions of secondary pigment cells (SP) between the crystalline cones (CC) are pigment-free. **F:** Electron micrograph of longitudinal section through a secondary pigment cell profile (SP), with accompanying pigment containing compartments between the crystalline cones (CC) in the dorsal eye. **G:** Same in cross-section. **H:** In the dorsal eye, secondary pigment cell nuclei (nSP) are associated with black pigment granules. **I:** Secondary pigment cell extensions are anchored to the primary pigment cell layer (PP), close to the nuclei of primary pigment cells (nPP). **J:** Electron micrograph of a longitudinal section through a secondary pigment cell anchor. Inset shows a cross-section with microtubules. Male, carapace width 1.7 cm.

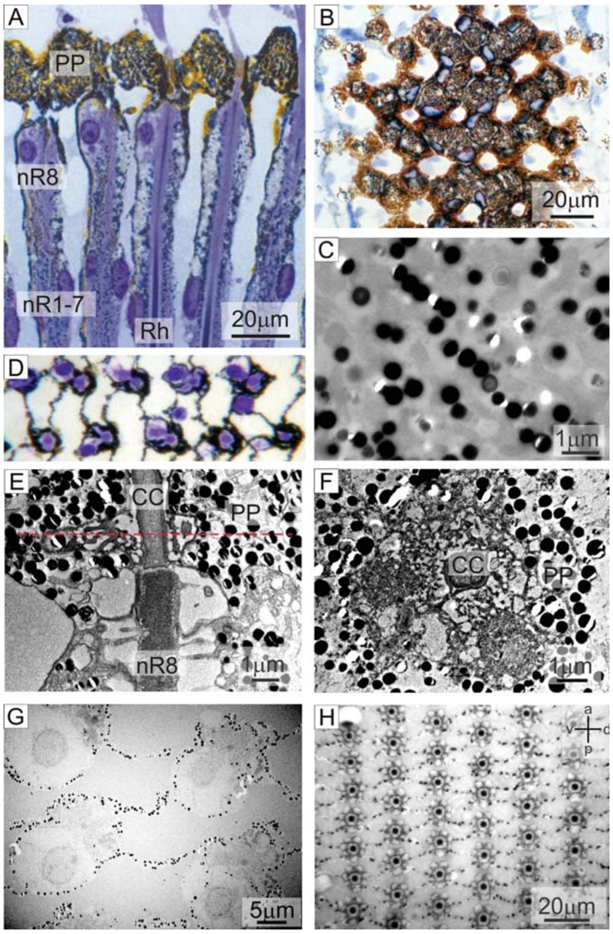

Figure 7. The primary pigment cells of *U. vomeris*. **A:** Light micrograph of a longitudinal section through the primary pigment cell layer (PP) and the distal retinular cell R8. nR8: nucleus of R8; nR1-7: nuclei of retinular cells R1–R7; Rh: Rhabdom. **B:** Light micrograph of a cross-section through the primary pigment cell layer. **C:** Electron micrograph of pigment granules in the primary pigment cell layer. Note differences in electron densities. Some pigment granules have fallen out of the section, leaving a white hole. **D:** Light micrograph of a cross-section at the level of the R8 nucleus, showing the distribution of primary pigment cell pigment at this level. **E:** Electron micrograph of a longitudinal section through the crystalline cone–R8 interface. Red dashed line indicates the level of the cross-section shown in (F). **F:** Cross-section through the most proximal part of the crystalline cone. Note primary pigment cell screening pigments retreating from the light path. **G,H:** Further along the proximal ommatidium, primary pigment cells form thin pigment filaments stretching between ommatidia. Male, carapace width 2.3 cm.

this level (Fig. 10A), a role that is most clearly seen a bit further down the rhabdom (Fig. 10C). Desmosomes mark the corners where the cell membranes of different cells meet (marked by white stars in Fig. 10A,C,E). The microvilli in the distal part of R8 are not arranged in parallel but form an irregular pattern of microvillar directions (Figs. 8C, 10A,C,D). The microvillar directions of pairs of facing lobes are similar (see lobes a and c in Fig. 10C). Scrambling of microvillar directions does not appear to be achieved by rotation of the lobes of R8 around the rhabdom. Scrambling rather takes the form of packets of microvilli being diverted away from the usual orientation perpendicular to the long axis of the rhabdom, assuming orientations nearly parallel to that axis. As a consequence, about half the microvilli in the R8 rhabdom are seen as round profiles in cross-sections through ommatidia (Fig. 10C). The microvillar directions in the proximal part of R8 become orthogonally aligned (Fig. 8D; see also Eguchi and Waterman, 1973).

The R8 lobes and the extensions of retinular cells R1–R7 contain many mitochondria throughout the cytoplasm and the cytoplasm of R8 contains widely distributed vacuoles throughout (Fig. 10E). These vacuoles appear empty and bright in electron-microscope sections and thus are likely to contain low-density material. They tend to form a narrow ring or palisade (peri-rhabdomal vacuole or palisade) around the rhabdom of R8, with a width of less than 1 μm (Fig. 10A,C,E). The cell body of R8 does not contain any pigment granules, but is surrounded by an electron-dense pigment granule screen formed by the primary pigment cells (Figs. 10B, 11). Towards the proximal end of R8, the lobes of R8 become very narrow (Figs. 10E,F, 11) and eventually fuse to form the R8 axon, which runs parallel to and at the periphery of the profiles of R6 and R7 down to the basement membrane (Fig. 11). At the same level, the extensions of retinular cells R1–R7 contain dense screening pigment granules, which, however, are positioned far away from the rhabdom (Figs. 10F, 11).

At the level of nuclei of retinular cells R1–R7, there is a smooth transition from the rhabdom of R8 to the main rhabdom to which R1 and R7 contribute microvilli. In longitudinal sections, this transition is marked by four changes (Figs. 8E, 9, 11): 1) microvillar directions become aligned in horizontal and vertical directions (e.g., Fig. 8D,F); 2) the palisade vacuole becomes wider (Fig. 8E); 3) screening pigment granules come to lie close to the outer circumference of the peri-rhabdomal vacuole; and 4) the main rhabdom has a larger diameter compared to the rhabdom of R8.

The microvilli of R1–R7 are oriented perpendicular to each other and are organized in alternating bands (Figs. 8F, 12). The main rhabdom has a square cross-section, one side of which is occupied by retinular cell R7 (Fig. 12A–D). With respect to eye coordinates, the microvilli in R3, R4, and R7 are aligned horizontally and those in R1, R2, R5, and R6 are aligned with the vertical. This can be verified by noting the lateral position of R7 in ommatidia in vertical light-microscopy cross-sections (Fig. 12A,B) and by the alignment of microvilli in

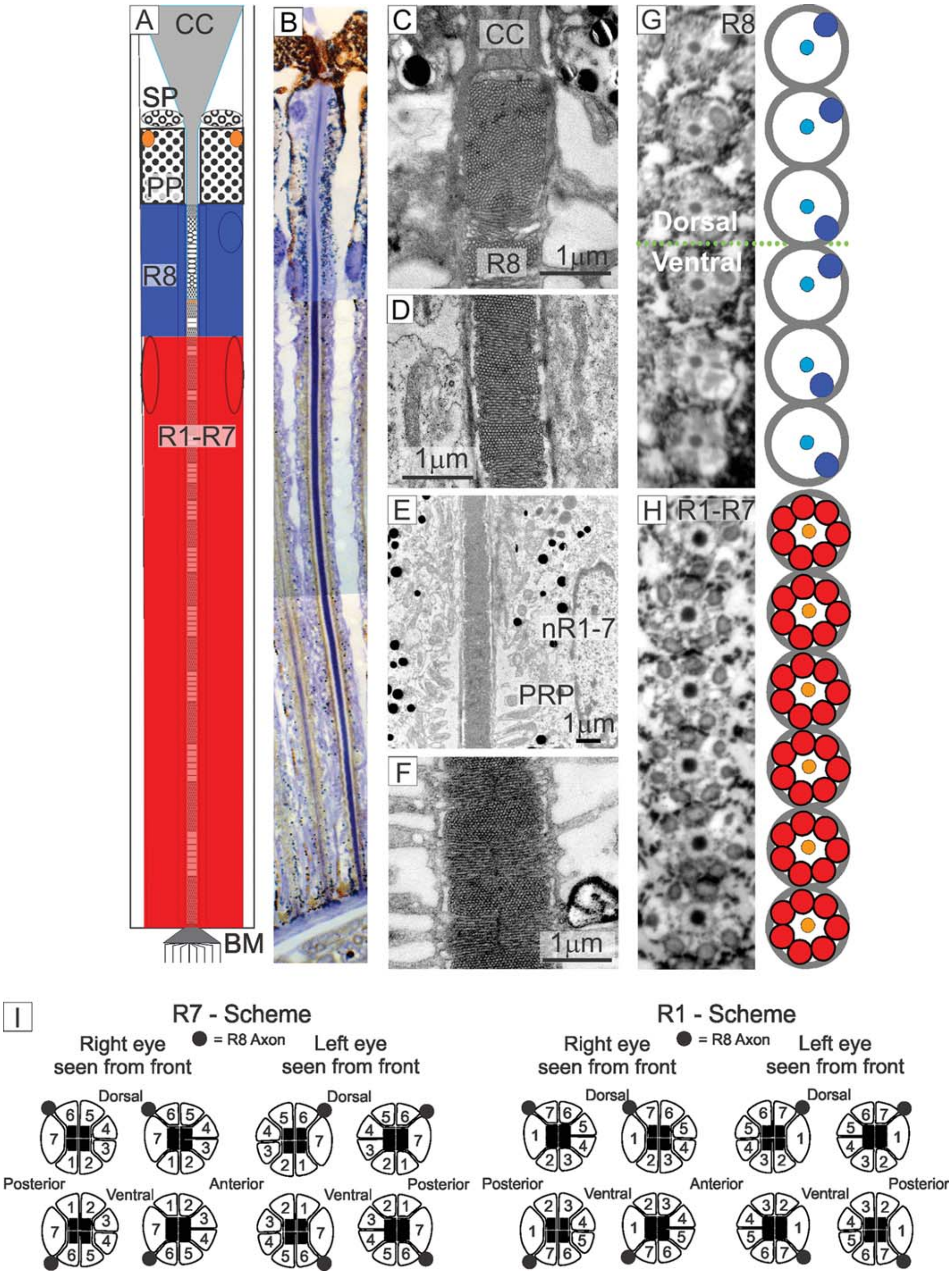

Figure 8. Overview of the ommatidium organization of *U. vomeris*. **A:** Schematic drawing of a longitudinal section through the ommatidium CC: Crystalline cone; SP: Secondary pigment cells; PP: Primary pigment cells; R8: Distal retinular cell R8 (R8 nucleus in dark blue); R1–R7: Proximal retinular cells R1–R7 (nuclei of R1–R7 in dark red); BM: Basement membrane. **B:** Equivalent light micrograph of a longitudinal section through the ommatidium. **C:** Electron micrograph of a longitudinal section through the crystalline cone tip (CC)–retinular cell R8 interface showing distal non-uniform microvillar directions in R8. **D:** Banded part of the proximal R8 rhabdom. **E:** Electron micrograph of a longitudinal section along the transition from the R8 to the R1–R7 rhabdom at the level of the R1–R7 nuclei (nR1–R7). Note widening of the peri-rhabdomal palisade (PRP) at this level. **F:** Electron micrograph of a longitudinal section through the rhabdom of R1–R7 showing alternating bands of horizontal and vertical microvilli. **G:** Light micrograph of a frontal cross-section of the left eye at the level of the R8 nucleus. The eye equator is defined by a switch in position of the R8 nucleus from dorsal of the rhabdom to ventral of the rhabdom (see schematic diagram on the right and in (I)). **H:** Light micrograph of a frontal cross-section at the level of R1–R7 nuclei, showing that nuclei all lie in one plane. Male, carapace width 2.3 cm. **I:** Schematic drawings of retinular cell numbering systems currently in use. The R7-scheme is used here and justified in the Materials and Methods section (see also Shaw and Stowe, 1982).

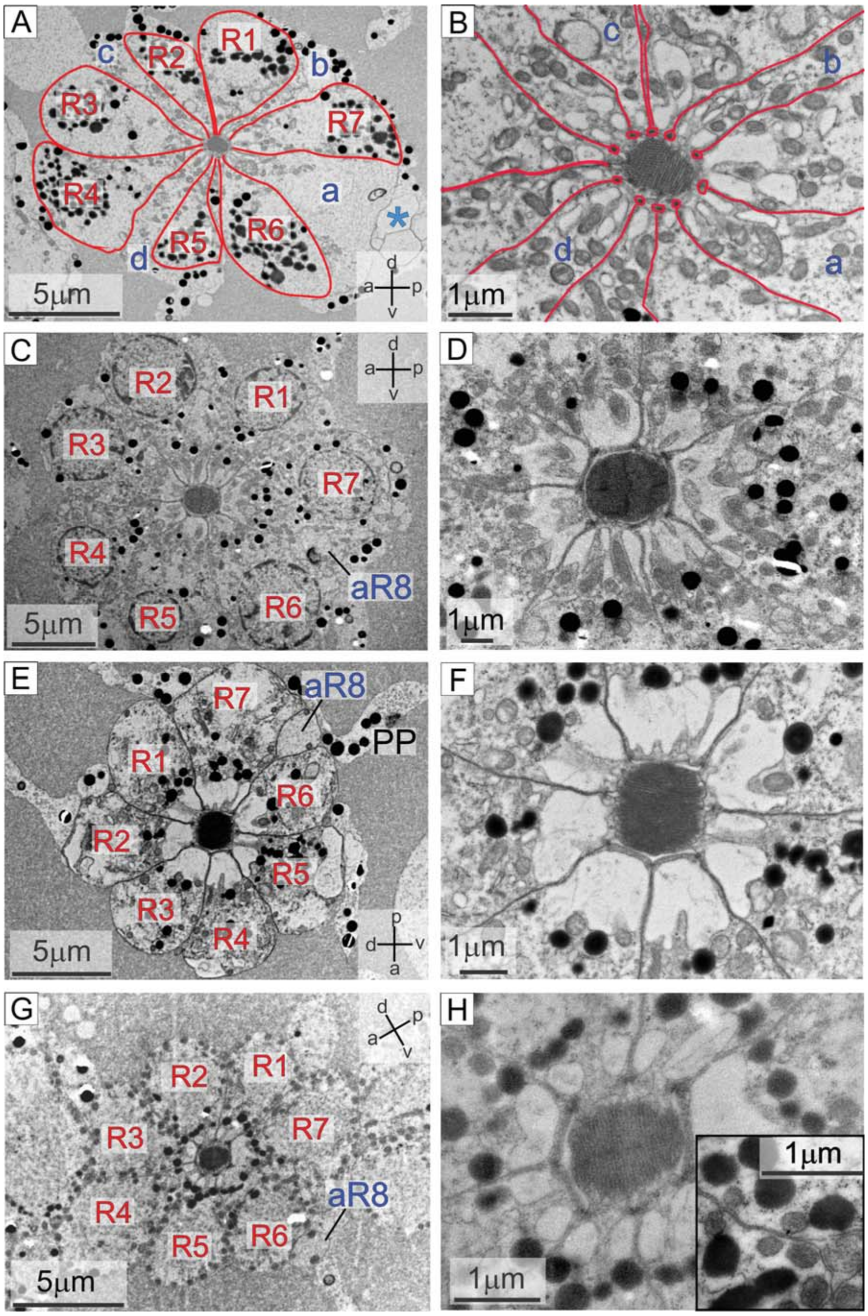

Figure 9. Overview of retinular cells in *U. vomeris*. Electron micrographs of cross-sections through retinular cell R8 at low magnification **(A)** and high magnification **(B)**. The four lobes of R8 are labeled a–d, which are pigment-free, but are surrounded by black pigment granules in the primary pigment cells. The four lobes are separated by distal extensions of retinular cells R1–R7, which contain black screening pigments. **C–H:** Electron micrographs of cross-sections through retinular cells R1–R7 at low magnification (C,E,G) and high magnification (D,F,H) from distal (top) to proximal (bottom). C,D: Cross-section through the nuclear region of the retinular cells of R1–R7. aR8: axon of R8. E,F: Cross-section through the medial part of the rhabdom. G,H: Cross-section through the proximal part of the rhabdom, where the pigment screen around the vacuole palisade becomes very dense. Inset in (H) shows dense arrangement of mitochondria. Male, carapace width 2.3 cm.

electron-microscopy cross-sections through the rhabdom (Fig. 12C–E). Within the ommatidium, retinular cells R1, R2, and R7 thus lie in a lateral position relative to the rhabdom, retinular cells R5 and R6 lie dorsal and R1 and R2 lie ventral of the rhabdom.

Figure 12C shows a cross-section through a band of horizontal microvilli from R3, R4, and R7, where R1, R2, R5, and R6 are prevented from contributing microvilli to the rhabdom at this level by a wide gap between the cell membranes of microvilli-contributing and

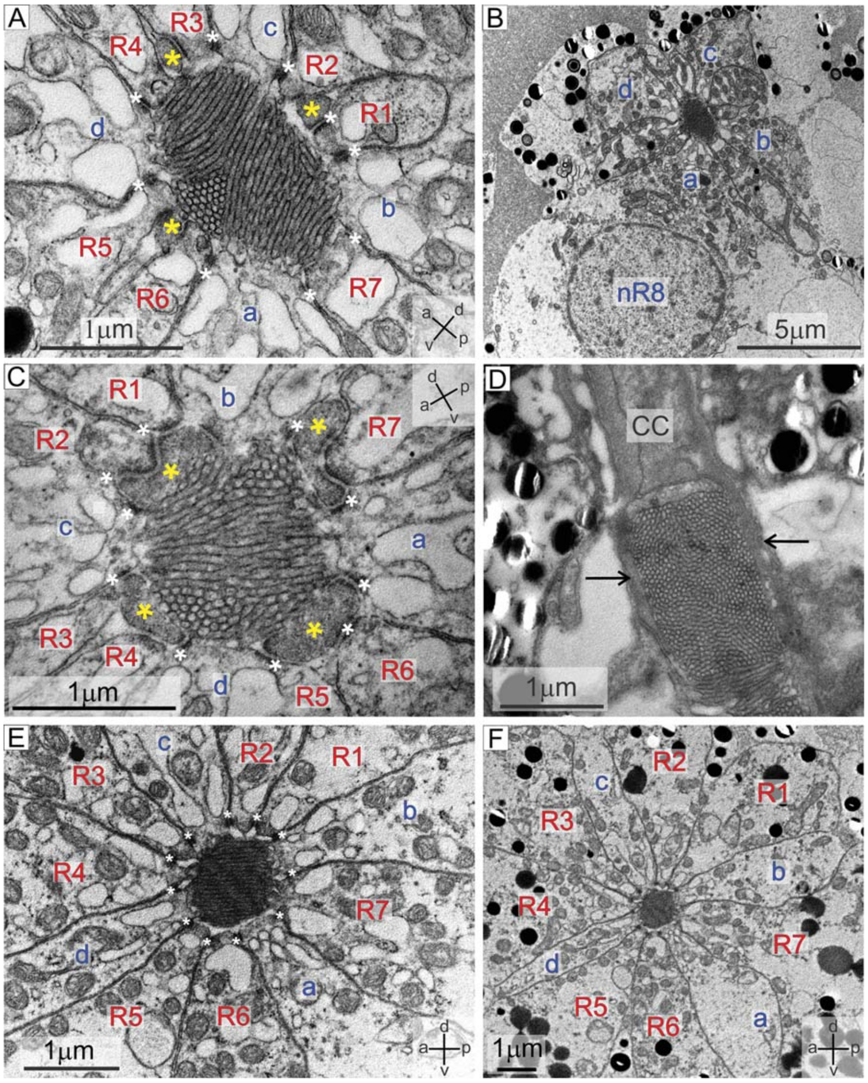

Figure 10. The retinular cell R8 of *U. vomeris*. **A:** Electron micrograph of a cross-section through the distal part of retinular cell R8 at the level of the R8 nucleus (nR8) (see same section at low magnification in **(B)**). Microvilli are contributed by the four lobes of R8 (blue, a–d), which are separated by distal extensions of the retinular cells R1–R7 (red), which are anchored to the rhabdom by proximal extensions of the crystalline cone cells (marked by yellow stars). Desmosomes at the cell borders are marked by white stars. Note large number of mitochondria in all cell profiles at this level. Male, carapace width 2.3 cm. **C:** Electron micrograph of a cross-section halfway along the retinular cell R8. The four lobes of R8 are separated by four flat extensions of the crystalline cone cells (yellow stars), which oppose the distal extensions retinular cells R1–R7 (red letters). The R8 lobes and the R1–R7 profiles are connected by desmosomes close to the rhabdom (marked by white stars). **D:** Electron micrograph of a longitudinal section through the crystalline cone–R8 interface, showing the crystalline cone extensions (arrows) hugging the rhabdom. **E:** EM cross-section through the R8–R1–R7 transition just distal to the level of R1–R7 nuclei. The rhabdom at this level shows horizontal microvilli which appear to be contributed by R8. Desmosomes are marked by white stars. Note large numbers of mitochondria in all cell profiles. **F:** Same as (E) at lower magnification. Note screening pigment granules, located away from the rhabdom in the retinular cells of R1–R7. Male, carapace width 2.3 cm.

noncontributing cells (marked by arrows in Fig. 12E). Figure 12D,E shows cross-sections through the main rhabdom at a level where R1, R2, R5, and R6 contribute microvilli to the rhabdom and where R3, R4, and R7 in turn are prevented from contributing to the rhabdom by a gap with thickened cell membranes. In other words, in those places where retinular cells R1–R7 contribute microvilli to the main rhabdom, the microvilli-lacunae interface consists of a single cell membrane, while a thick space between two cell membranes prevents other retinular cells from contributing microvilli to the rhabdom (Fig. 12E). Desmosomes mark the boundaries between the retinular cells (white stars in Fig. 12E).

The banding pattern of perpendicular microvillar directions in fiddler crab rhabdoms varies systematically along the length of the rhabdom (see Fig. 15) and the

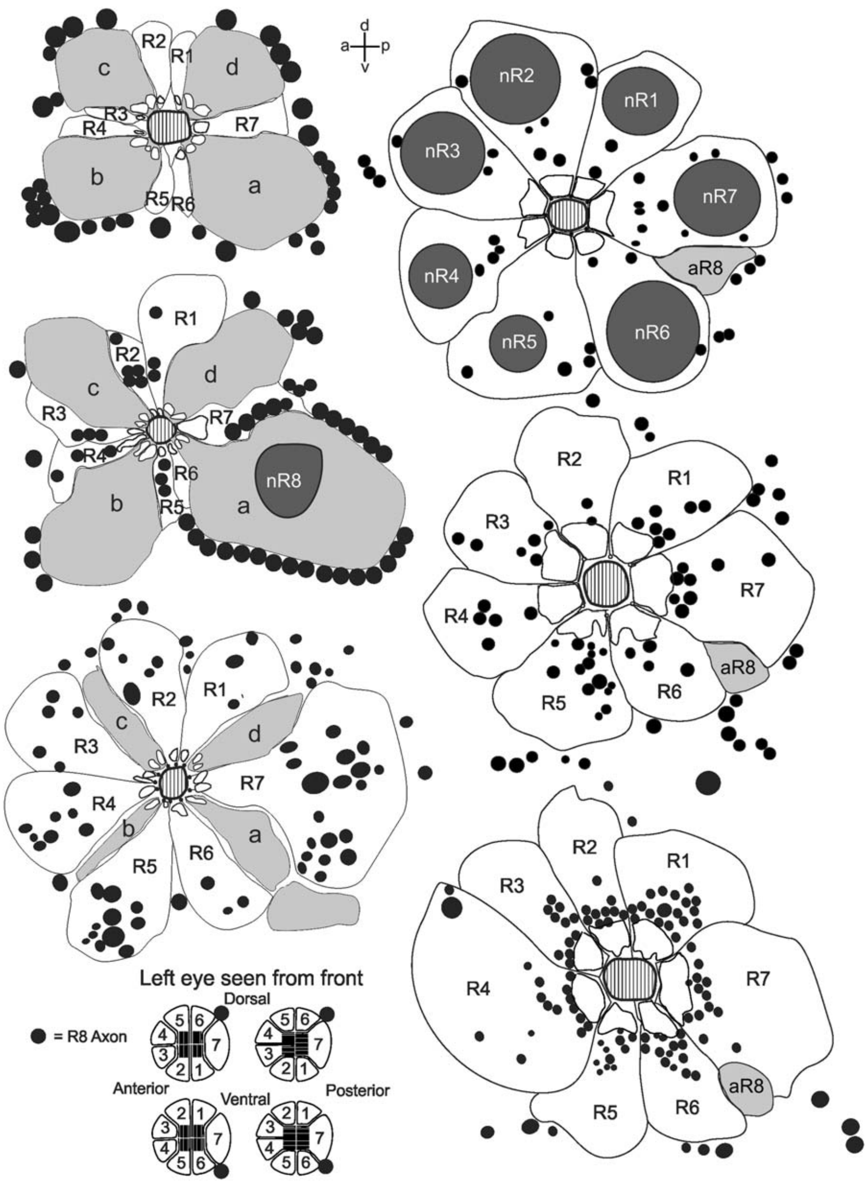

Figure 11. Drawings of cross-sections through the *U. vomeris* ommatidium. Representative sections looking into the ventral half of the left eye (see schematic at bottom right) are drawn from distal (top left) to proximal (bottom right). The cell body partitions of R8 are shaded light gray and nuclei in dark gray. nR8: nucleus of R8; aR8: axon of R8; nR1–R7: nuclei of R1–R7. Black circles are pigment granules.

banding pattern differs in different parts of the eye. We have documented and discussed the regional variations of this banding pattern elsewhere (Alkaladi et al., 2013).

Distribution of screening pigments in retinula cells

In contrast to retinular cell R8, which does not contain any pigment granules, retinular cells R1–R7 contain at least two kinds of pigments. This can be seen in light-microscopy cross-sections at the level of R8 (Fig. 13A) and slightly lower, at the level of the nuclei of R1–R7 (Fig. 13B). In the most distal part of R1–R7, retinular cells contain dense black pigment throughout the extensions they send distally between the lobes of retinular cell R8 (Figs. 10F, 13A,B). At the level of R1–R7 nuclei, retinular cells contain pigment that appears orange-golden in histological sections and is located distal to the nuclei (Fig. 13G,H) and then close to the outer circumference of the peri-rhabdomal lacunae (Fig. 13C,D). At this level, the orange-golden pigment is mixed with black pigment. In the proximal part of the rhabdom, the peri-rhabdomal palisade is densely surrounded by this orange-golden pigment (Fig. 13C) that appears red in cryostat sections (inset Fig. 13C; see also Jordão et al., 2007). Electron-microscopy cross-sections show mostly round black (electron-dense)

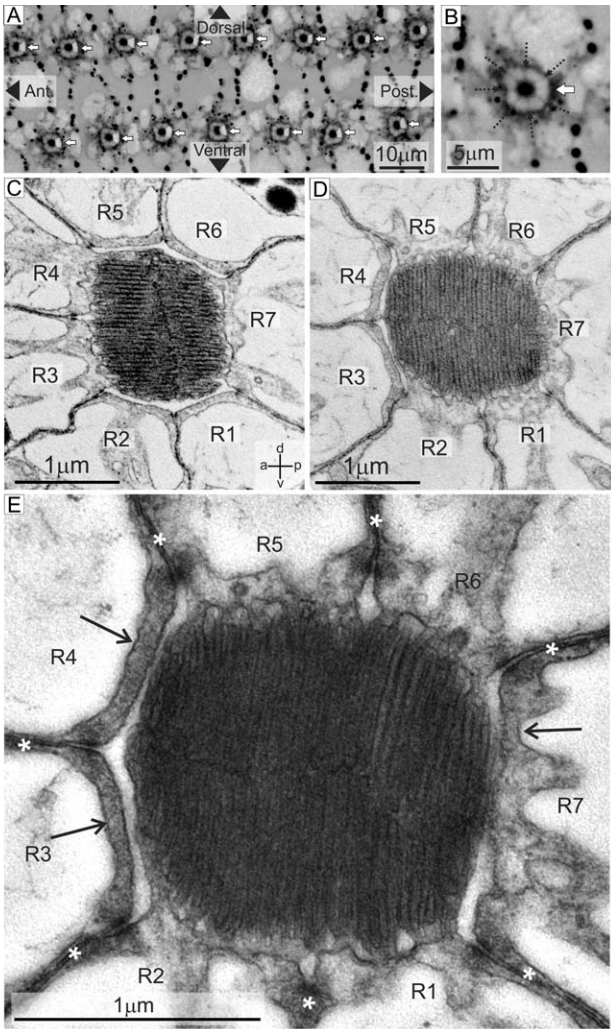

Figure 12. The rhabdom of retinular cells R1–R7 in *U. vomeris*. **A:** The position of retinular cell R7 in the ommatidial array. Light micrograph of a frontal section through the ommatidial array of the left eye close to the eye equator at the level of the main rhabdom. The position of R7 (white arrows) is highlighted. **B:** Enlarged image of a single ommatidium showing the cell boundaries crossing the peri-rhabdomeral palisade (black arrows) that can be used to determine the location of R7 (white arrow) in light microscopy sections. Male, carapace width 2.32 cm. **C:** Electron micrograph of a cross-section through a microvillar band of the main rhabdom in the dorsal part of the left eye, in which retinular cells R3, R4, and R7 contribute horizontally aligned microvilli to the rhabdom. The other retinular cells are separated from the rhabdom by a thickened cell membrane. **D:** Same as (C) at a level where the retinular cells R1, R2, R5, and R6 contribute the vertically oriented microvilli to the rhabdom. **E:** The main rhabdom at higher magnification at a level where retinular cells R1, R2, R5, and R6 contribute vertically oriented microvilli to the rhabdom. Arrows point to thickened cell membranes of retinular cells R3, R4, and R7; desmosomes at the border between retinular cells are marked by white stars. Male, carapace width 2.3 cm.

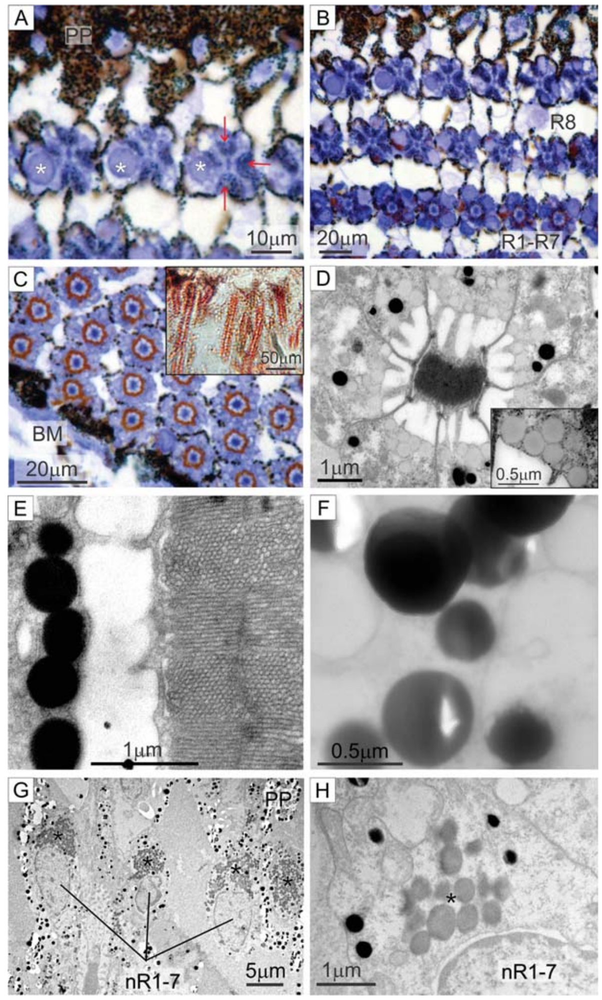

Figure 13. Distribution of screening pigments in the retinular cells of *U. vomeris*. **A:** Light micrograph of a cross-section at the level of the R8 nucleus (marked by white stars). Red arrows point to screening pigment in the distal extensions of retinular cells R1–R7. **B:** Light micrograph of a cross-section through three rows of ommatidia in the transition between R8 and R1–R7. Note black and gold-orange pigment granules close to the peri-rhabdomal palisade. **C:** Light micrograph of a cross-section through the most proximal part of ommatidia, close to the basement membrane (BM). Inset shows the color of pigments in a cryostat section. Male, carapace width 2.3 cm. **D:** Electron micrograph of a cross-section through the rhabdom of the dorsal eye showing two types of pigment granules with different electron densities. Inset shows enlarged image of less electron-dense granules. Male, carapace width 2.3 cm. **E:** Electron micrograph of a longitudinal section through the rhabdom showing electron dense pigment granules hugging the peri-rhabdomeral palisade. **F:** Two types of pigment granules in primary pigment cells at high magnification. The electron-dense granules are contained in a membrane that appears less electron-dense. Less electron-dense granules do not appear to have a membrane. **G:** Packages of less electron-dense pigment granules (marked by black stars) just distal to the nuclei of R1–R7. **H:** Enlarged views of these pigment granule assemblies. Note the distinct difference of these pigment granules compared to the very electron-dense black granules of the second type. G,H: Male, carapace width 2.9 cm.

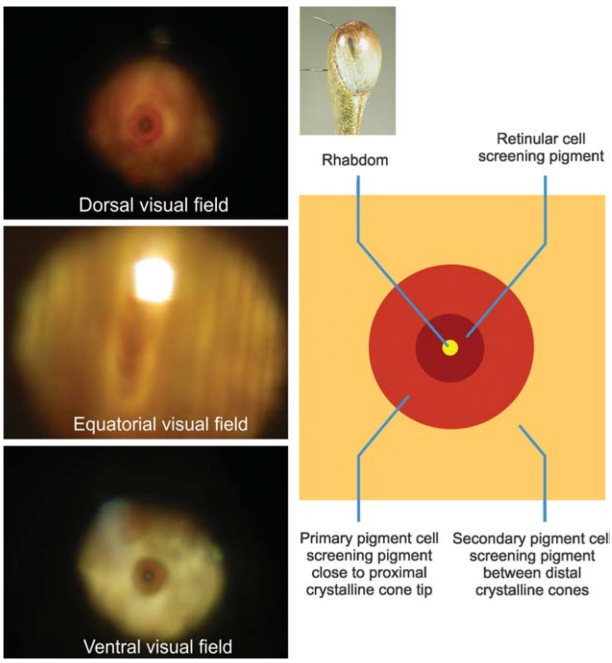

Figure 14. The color of screening pigments in the live eye. Light micrographs on the left show deep pseudopupils under orthodromic illumination in the dorsal, equatorial, and ventral part of the *U. vomeris* eye. Deep pseudopupils are enlarged, superimposed virtual images of the rhabdom and the pigment cells in the back focal plane of each lens. The different components of the deep pseudopupil are explained in the schematic drawing on the right. Inset photograph shows the eye under normal illumination.

pigment granules with a clearly defined, sharp edge (Fig. 13E). However, there clearly are pigment granules of a second type, that are less electron-dense and therefore appear gray (Fig. 13D,F). At high magnification, their edge compared to that of electron-dense granules appears less well defined (Fig. 13F). Their ultrastructure in electron microscopy sections and their orange-golden appearance in light microscopy sections thus suggests that they are formed by lipids (see also Jordão et al., 2007).

It is hard to be sure to what extent the colors of pigments in compound eyes are being modified by the histological procedures of fixation and dehydration (e.g., Marshall et al., 2001). However, the true colors of both screening pigments in retinular cells and in pigment cells can be verified *in vivo* by observing the deep pseudopupil under orthodromic illumination (Fig. 14). The deep pseudopupil is an enlarged, virtual, superimposed image of the structures in the back focal plane of facet lenses (see Franceschini, 1975; Stavenga, 1979). In the case of the fiddler crab eye the deep pseudopupil shows the pigment around the rhabdom as dark brown (see schematic diagram in Fig, 14), the primary pigment screen around the proximal crystalline cone tip as red in the dorsal eye and light brown in the ventral eye and the secondary pigment screen between the crystalline cones as yellow-red (dorsal), yellow-orange (equatorial) and pale-yellow (ventral).

DISCUSSION

Fiddler crabs have typical apposition compound eyes, which in many aspects conform to the general pattern that has been described for other decapod crustaceans (e.g., Shaw and Stowe, 1982; Rosenberg et al., 2001). We have documented this on the light- and the electron-microscopy level and summarize our findings in the schematic images in Figure 15. However, we also discovered a number of specializations in the fiddler crab compound eye, which may or may not be unique to this particular genus of crabs.

We confirm that the dimensions of ommatidial components vary in the different parts of the eye (Zeil and Al Mutairi, 1996). While the diameter of both R8 and R1–R7 rhabdoms remains constant, rhabdoms and crystalline cones are longer and the diameter of facet lenses is larger along the eye equator than in the rest

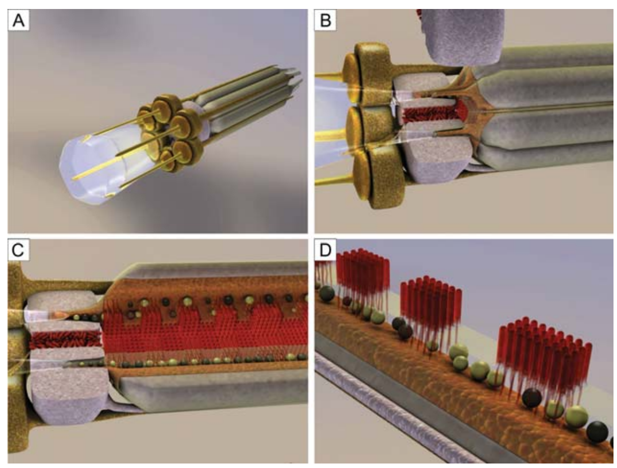

Figure 15. Summary graphics of the *U. vomeris* ommatidium. **A:** Schematic image of one isolated ommatidium, showing the dorsal eye pattern of secondary pigment cells (light gold), the six primary pigment cells (dark gold) and the retinular cells (gray). **B:** Cut-away schematic image of the crystalline cone-R8-R1–R7 interface. Microvilli are shown in red. **C:** Schematic detail of the R8 and the R1–R7 rhabdom, indicating the interdigitating arrangement of microvilli bands in R1–R7. Retinular cell screening pigment granules are shown as dark and light golden spheres. **D:** Schematic image of one isolated retinular cell with microvillar bands of increasing length from distal (left) to proximal (right). For details of microvillar banding patterns, see Alkaladi et al. (2013). Artwork by Sharyn Wragg, The Australian National University, and Thomas Maghill, Canberra (see http://biology.anu.edu.au/jochen_zeil/crab_eye_tutorial/).

of the eye, reaching maximal dimensions in the lateral part of the visual field. The large diameters of the facet lenses at the eye equator mean that in this part of the eye both sensitivity and resolution are higher than in the rest of the eye. The very long rhabdoms further increase sensitivity at the eye equator, while the long crystalline cones have the opposite effect. The increased focal length leads to smaller acceptance angles, which decreases sensitivity, but increases resolution (Warrant and McIntyre, 1993; Smolka and Hemmi, 2009).

As far as the optics are concerned, fiddler crab ommatidia have flat lenses, most probably a witness to their aquatic past, where the minimal refractive index difference between water and cuticle made the cuticle-water interface ineffective for focusing. We showed that the corneal facet lenses on their own are sufficient and do not require crystalline cones to focus light because the lenses themselves produce an image in the appropriate distance. Focusing power thus must be produced by a refractive index gradient inside the lens. It will be interesting to see whether other amphibious and terrestrial crustaceans have also retained this design of their optical system that provides identical refraction in air and in water, or whether they have evolved curved cuticular lenses to exploit the air–cuticle interface as a seemingly more effective means of focusing light onto the rhabdom.

We identified different types of pigment granules in the fiddler crab eye, which differ in electron-density, in size and in color, both in histological preparations and *in vivo*. Elofsson and Hallberg (1973) investigated the ultrastructure of pigment granules in the eyes of *Crangon crangon*, showing that different pigment granules are associated with three different chromatophores containing black, white, and red pigments. Elofsson and Kauri (1971) reported that black chromatophore granules are electron-dense and are surrounded by a membrane, although the membrane is difficult to observe. The pigment granules in the red chromatophores do not have membranes and are less electron-dense. Like the yellow pigments, the white chromatophores contain empty granules. The average size and the chemical composition of the pigment granules in cuticular chromatophores and in the pigment cells of the eye are similar.

As we have shown, the fiddler crab ommatidium contains a variety of screening pigments, which, depending on their location and their color, are likely to play a number of different roles (see Stavenga, 1979). Pigments in primary cells are typically positioned to ensure that light enters the ommatidium through its own lens parallel to its optical axis and that stray light entering the eye from other directions is absorbed. We found two types of pigment granules in the primary pigment cells, distinguished by their electron density that appear black and golden in histological sections when viewed in the light microscope and dark-red to brown in the intact eye (Fig. 14).

The location and shape of secondary pigment cells differs in the dorsal, the equatorial, and ventral parts of the eye. In the dorsal eye, the elongated secondary pigment cells form narrow pigment screens running between the crystalline cones parallel to their long axis. They appear dark brown in the intact eye (Fig. 14). These screens are likely to function as sun- and skylight blinds, preventing high-intensity light from above to scatter within the crystalline cone tract and to reach rhabdoms from directions other than through the individual lenses of ommatidia. Fiddler crabs, who operate on exposed tropical and subtropical mudflats during daylight low tides, may be uniquely exposed to high-intensity light from above and therefore may have a particular need for such blinds, but it may be worth investigating whether dorsoventral screening pigment specializations of this kind are not more common in Arthropods.

In the equatorial and ventral eye, the secondary pigment cells take on other functions. Their profiles between the crystalline cones are pigment free and their nuclei lie just distal to the primary pigment cell layer in long perpendicular extensions of the cells, which run just distal to and parallel to the primary pigment cell layer. These proximal extensions of secondary pigment cells form pigment compartments distal from the primary pigment cell layer, which contain pigment granules of different sizes, shapes, and electron densities. The secondary pigment compartments screen from view from the outside the primary pigment cells, which form a thick, dark brown pigment layer where the proximal tips of crystalline cones and the distal tips of the rhabdom meet (Fig. 14). These secondary pigment screens are responsible for the fact that the equatorial and ventral parts of fiddler crab eyes do not appear dark to the observer (see Figs. (1 and 14)) and one of their functions may therefore be to camouflage the underlying primary pigment layer. However, because these pigment compartments contain bright and strongly reflecting pigment granules, they may also reflect long-wavelength light or even infrared wavelengths and therefore prevent heat absorption by the underlying black pigment. It would be very interesting to measure the spectral composition of light reflected by secondary pigment cells and to measure the heat reflected from the dorsal and the ventral eye with a heat-sensitive camera.

As far as the retinular cells in fiddler crab compound eyes are concerned, we identify three properties that are functionally important, but little understood: the distribution of screening pigments, the dimensions of peri-rhabdomal vacuole palisades, and the variations of microvillar banding patterns along the length of the rhabdom (Alkaladi et al., 2013). First, it is noticeable that the retinular cells R8 are free of screening pigments granules, like in crayfish (Krebs and Lietz, 1982) and grapsid crabs (Eguchi and Waterman, 1973), while retinular cells R1–R7 contain at least two kinds of pigment granules, which have the same size, electron-densities, and golden-black color when viewed in the light microscope as the ones in the primary pigment cells. In cryosections, these pigments appear bright red (Fig. 13C) and in the intact eye, dark brown (Fig. 14). Most important, however, screening pigment granules form a tight ring around the vacuole palisade of the main rhabdom, but never lie close to the rhabdom itself. Given that the main rhabdom has a diameter of about 2 μm and is surrounded by a vacuole palisade of about the same width, the waveguide or light-guide properties of this arrangement and the functional significance of the red-brown pigment screen are far from clear. It has so far been assumed (e.g., Jordão et al., 2007) that colored screening pigment close to the rhabdom may absorb and modify the spectral composition of light traveling along, and partially outside the rhabdom in distinct modes. Given the relatively large diameter of the high-refractive index rhabdom and of the surrounding low-refractive index palisade, however, light traveling outside the rhabdom would appear to be fully contained within the vacuole palisade (Stavenga, 2003a). The screening pigment hugging the outer wall of the vacuole palisade may thus not interact with light traveling along the rhabdom, but rather provide a screen against light entering from the outside. However, we may have missed one important property of the peri-rhabdomal vacuole: Marshall et al. (1991) found in mantis shrimps that the palisade contains colored pigment, which can only be seen in frozen sections. This indicates that the pigment is lipid-based and is washed out by alcoholic solvents that are used to dehydrate the tissue for normal histological analysis. We have checked frozen sections of *U. vomeris* compound eyes (see inset Fig. 13C), but could not see evidence of color in the palisade.

A full appreciation of the adaptive significance of the distribution and color of screening pigments, the dimensions of rhabdom and palisade vacuole, and the arrangement of microvilli in fiddler crab compound eyes will require wave- and light-guide modeling, as has been done recently for insect eyes (Stavenga 2003a,b).

Considering what is known about the microvillar arrangement in the different retinular cells in crustacean compound eyes, it came as no surprise to find that microvillar directions in the distal part of retinular cell R8 are not uniform in fiddler crabs and that microvilli in the main rhabdom are arranged in distinct, alternating bands of perpendicular directions (e.g., Eguchi and Waterman, 1973; Shaw and Stowe, 1982). However, in fiddler crabs at least, bands become increasingly longer along the length of the rhabdom (Alkaladi et al., 2013), as has been briefly noted once before in Euphausids (Meyer-Rochow and Walsh,1978).

To discuss first the microvillar arrangement in retinular cell R8, we note that the variation of microvillar direction along the length of the rhabdom is not achieved by a rotation (twisting) of the four lobes of R8 which contribute microvilli to the rhabdom, but by discrete packets of microvilli assuming directions nearly parallel, rather than perpendicular, to the long axis of the rhabdom. As far as microvillar arrangement is concerned, the properties of R8 in fiddler crabs are thus similar to what has been found in pelagic shrimps (*Acetes sibogae*: Ball et al., 1986). As a consequence, R8 is unlikely to be sensitive to the plane of polarization of light, but may rather be part of a color vision channel in the fiddler crab eye. This possibility has been raised a number of times before, because electroretinogram recordings in fiddler crabs indicate the presence of two visual pigments (Horch et al., 2002), because R8 has been shown to be a violet receptor in crayfish (Cummins and Goldsmith, 1981), and because *in situ* hybridization has shown that a UV-sensitive opsin-encoding gene is only expressed in the R8 receptors of *Uca pugilator* (Rajkumar et al., 2010).

The compound eyes of fiddler crabs are oval in shape, with a vertical long axis, and their hexagonal facet array is of the standing type (e.g., Zeil et al., 1986), with facet rows being perfectly horizontal at the eye equator. We were thus able to determine the arrangement of the microvilli relative to the facet array for the main rhabdom. The retinular cells R3, R4, and R7 have lateral positions in the ommatidium and contribute horizontal microvilli relative to the orientation of the facet array and the orientation of the eye. Retinular cells R1, R2, R5, and R6 contribute vertical microvilli to the main rhabdom, with R1 and R2 occupying the ventral positions and R5 and R6 the dorsal positions in the ommatidium.

In functional terms the most challenging aspect of microvillar organization in the fiddler crab rhabdom, however, is the fact that rhabdom banding patterns change systematically along the length of the rhabdom and that banding patterns differ in different parts of the eye (Alkaladi et al., 2013). In the main rhabdoms, microvillar bands increase in length from distal to proximal (see Fig. 15) and modeling photon absorption indicates that this arrangement leads to photon absorption probability remaining constant along the length of retinular cells (Alkaladi et al., 2013). Moreover, in the rhabdoms of the dorsal eye, horizontal microvilli occupy only half the cross-sectional area as vertical microvilli, which reduces the absorption of horizontally polarized light and increases the difference between absorption in retinular cells with horizontal and vertical microvilli.

ACKNOWLEDGMENTS

We thank Peter McIntyre and Eric Warrant for showing us how to carry out the hanging drop experiments. We thank Sally Stowe and Willi Ribi for histological advice, Carsten Müller for advice with the numbering of retinular cells and Doekele Stavenga, not only for assembling an epi-illumination microscope, but also for help with interpreting the deep pseudopupil in fiddler crabs. We acknowledge support from the EM Units at the Research School of Biology and the John Curtin School of Medical Research at the ANU and from Prof. Abdulrahman Al-Youbi, King Abdulaziz University.

CONFLICT OF INTEREST

There are no conflicts of interest.

ROLE OF AUTHORS

Both authors had full access to all the data in the study and take responsibility for the integrity of the data and the accuracy of the data analysis. Study concept and design: AA and JZ. Acquisition of data: AA. Analysis and interpretation of data: AA and JZ. Drafting of the article: AA. Critical revision of the article for important intellectual content: AA and JZ. Obtained funding: AA and JZ. Administrative, technical, and material support: AA and JZ. Study supervision: JZ.

LITERATURE CITED

Alkaladi A, How M, Zeil J. 2013. Systematic variations in microvilli banding patterns along fiddler crab rhabdoms. J Comp Physiol A 199:99–113.

Arikawa K, Kawamata K, Suzuki T, Eguchi E. 1987. Daily changes of structure, function and rhodopsin content in the compound eye of the crab *Hemigrapsus sanguineus*. J Comp Physiol A 161:161–174.

Ball EE, Kao LC, Stone RC, Land MF. 1986. Eye structure and optics in the pelagic shrimp *Acetes sibogae* (Decapoda, Natantia, Sergestidae) in relation to light-dark adaptation and natural history. Philos Trans R Soc Lond B 313:251–270.

Crane J. 1975. Fiddler crabs of the world. *Ocypodidae*: Genus *Uca*. Princeton, NJ: Princeton University Press.

Cummins D, Goldsmith TH. 1981. Cellular identification of the violet receptor in the crayfish eye. J Comp Physiol 142: 199–202.

Dembowski J. 1913. Über den Bau der Augen von *Ocypode ceratophthalma* Fabr. Zool Jb Anat 36:513–524.

Eguchi E, Waterman TH. 1973. Orthogonal microvillus pattern in the eight rhabdomere of the rock crab *Grapsus*. Z Zellforsch 137:145–157.

Elofsson R, Hallberg E. 1973. Correlation of ultrastructure and chemical composition of Crustacean chromatophore pigment. Ultrastruct Res 44:421–429.

Elofsson R, Kauri T. 1971. The ultrastructure of the chromatophores of *Crangon* and *Pandalud* (Crustacea). Ultrastructure Res 36:263–270.

Franceschini N. 1975. Sampling of the visual environment by the compound eye of the fly: fundamentals and applications. In: Snyder AW, Menzel R, editors. Photoreceptor optics. Berlin, Heidelberg, New York: Springer. p 98–125.

Friedrich M, Wood EJ, Wu M. 2011. Developmental evolution of the insect retina: Insights from standardized numbering of homologous photoreceptors. J Exp Zool 316:484–499.

Hallberg E, Elofsson R. 1989. Construction of the pigment shield of the Crustacean compound eye: A Review. J Crust Biol 9:359–372.

Hafner GS, Tokarski TR. 2001. Retinal development in the lobster *Homarus americanus*. Comparison with compound eyes of insects and other crustaceans. Cell Tissue Res 305:147–158.

Harzsch S, Hafner G. 2006. Evolution of eye development in arthropods: phylogenetic aspects. Arth Struct Dev 35: 319–340.

Hemmi JM, Tomsic D. 2011. The neuroethology of escape in crabs: from sensory ecology to neurons and back. Curr Opin Neurobiol 22:1–7.

Horch K, Salmon M, Forward R. 2002. Evidence for a two pigment visual system in the fiddler crab, *Uca thayeri*. J Comp Physiol A 188:493–499.

Jordão JM, Cronin TW, Oliveira RF. 2007. Spectral sensitivity of four species of fiddler crabs (*Uca pugnax*, *Uca pugilator, Uca vomeris* and *Uca tangeri*) measured by *in situ* microspectrophotometry. J Exp Biol 210:447–453.

Krebs W, Lietz R. 1982. Apical region of the crayfish retinula. Cell Tissue Res 222:409–415.

Kunze P. 1967. Histologische Untersuchungen zum Bau des Auges von *Ocypode cursor (Brachyura*). Z Zellforsch Mikr Anat 82:466–478.

Kunze P, Boschek CB. 1968. Elektronenmikroskopische Untersuchungen zur Form der achten Retinulazelle bei *Ocypode*. Z Naturforsch 23b:568–569.

Land MF, Layne J. 1995. The visual control of behaviour in fiddler crabs I. Resolution, threshold and the role of the horizon. J Comp Physiol A 177:81–90.

Layne JE. 1998. Retinal location is the key to identifying predators in fiddler crabs (*Uca pugilator*). J Exp Biol 201: 2253–2261.

Layne J, Land MF, Zeil J. 1997. Fiddler crabs use the visual horizon to distinguish predators from conspecifics: a review of the evidence. J Mar Biol 77:43–54.

Marshall NJ, Land MF, King CA, Cronin TW. 1991. The compound eyes of mantis shrimps (Crustacea, Hoplocarida, Stomatopoda). II. Color pigments in the eyes of stomatopod crustaceans: polychromatic vision by serial and lateral filtering. Philos Trans R Soc Lond B 334:57–84.

Meinertzhagen IA. 1991. Evolution of the cellular organization of the Arthropod compound eye and optic lobe. In: Cronly-Dillon JR, Gregory RL, editors. Evolution of the eye and visual system. Basingstoke, UK: Macmillan Press. p 341–363.

Melzer RR, Diersch R, Nicastro D, Smola U. 1997. Compound eye evolution: Highly conserved retinula and cone cell patterns indicate a common origin of the insect and crustacean ommatidium. Naturwiss 84:542–544.

Melzer RR, Michalke C, Smolka U. 2000. Walking on insect paths? Early ommaditial development in the compound eye of the ancestral crustacean, *Triops cancriformis*. Naturwiss 87:308–311.

Meyer-Rochow VB, Walsh S. 1978. The eyes of mesopelagic Crustaceans. III. *Thysanopoda tricuspidata* (Euphausiacea). Cell Tiss Res 195:59–79.

Nilsson DE. 1990. Three unexpected cases of refracting superposition eyes in crustaceans. J Comp Physiol A 167:71–78.

Pope DS. 2005. Waving in a crowd: fiddler crabs signal in networks. In: McGregor PK, editor. Animal communication networks. Cambridge, UK: Cambridge University Press. p 252–276.

Rajkumar P, Rollmann SM, Cook TA, Layne JE. 2010. Molecular evidence for color discrimination in the Atlantic sand fiddler crab, *Uca pugilator*. J Exp Biol 213:4240–4248.

Ready DF. 1989. A multifaceted approach to neural development. Trends Neurosci 12:102–110.

Rosenberg MS. 2001. The systematics and taxonomy of fiddler crabs: a phylogeny of the genus *Uca*. J Crust Biol 21:839–869.

Rosenberg J, Langer H. 2001. Ultrastructural changes of rhabdoms of the eyes of *Ocypode* species in relation to different regimes of light dark adaptation. J Crust Biol 21: 345–353.

Rosenberg J, Henning U, Langer H. 2001. Diurnal changes of fine structure in the compound eyes of the ghost crab *Ocypode ryderi* (Crustacea, Decapoda, Ocypodidae). J Acta Biol Benrodis 11:53–70.

Shaw SR, Stowe S. 1982. Photoreception. In: Atwood HL, Sandeman DC, editors. The biology of Crustacea, vol III. New York: Academic Press. p 292–367.

Smolka J, Hemmi JM. 2009. Topography of vision and behaviour. J Exp Biol 212:3522–3532.

Smolka J, Zeil J, Hemmi JM. 2011. Natural visual cues eliciting predator avoidance in fiddler crabs. Proc Roy Soc Lond B 278:3584–3592.

Stavenga DG. 1979. Pseudopupils of compound eyes. In: Autrum H, editor. Handbook of sensory physiology, vol.-VII/6A. Berlin, Heidelberg, New York: Springer. p 357–439.

Stavenga DG. 2003a. Angular and spectral sensitivity of fly photoreceptors. I. Integrated facet lens and rhabdomere optics. J Comp Physiol A189:1–17.

Stavenga DG. 2003b. Angular and spectral sensitivity of fly photoreceptors. II. Dependence on facet lens F-number and rhabdomere type in *Drosophila*. J Comp Physiol A189:189–202.

Stowe S. 1982. Rhabdom synthesis in isolated eyestalks and retinae of the crab *Leptograpsus variegatus*. J Comp Physiol 148:313–321.

Toh Y. 1987. Diurnal changes of rhabdom structure in the compound eye of the grapsid crab, *Hemigrapsus penicillatus*. J Electron Microsc 39:492–500.

Warrant EJ, Kelber A, Wallén R, Wcislo WT. 2006. Ocellar optics in nocturnal and diurnal bees and wasps. Arthropod Struct Dev 35:293–305.

Waterman TH. 1981. Polarization sensitivity, In: Autrum H, editor. Handbook of sensory physiology. Heidelberg, New York: Springer. p 281–469.

Zeil J, Al-Mutairi MM. 1996. The variation of resolution and of ommatidial dimensions in the compound eyes of the fiddler crab *Uca lactea annulipes* (Ocypodidae, Brachyura, Decapoda). J Exp Biol 199:1569–1577.

Zeil J, Hemmi JM. 2006. The visual ecology of fiddler crabs. J Comp PhysiolA 192:1–25.

Zeil J, Hofmann M. 2001. Signals from crabworld: cuticular reflections in a fiddler crab colony. J Exp Biol 204:2561–2569.

Zeil J, Zanker JM. 1997. A glimpse into crabworld. Vision Research 37:3417–3426.

Zeil J, Nalbach G, Nalbach HO. 1986. Eyes, eye stalks and the visual world of semi-terrestrial crabs. J Comp Physiol A159:801–811.